ChemComm

COMMUNICATION

View Article Online
View Journal | View Issue

Cite this: *Chem. Commun.*, 2024, **60**, 1876

Received 17th November 2023,
Accepted 15th January 2024

DOI: 10.1039/d3cc05660k

rsc.li/chemcomm

Post transition metal substituted Keggin-type POMs as thin film chemiresistive sensors for H_2O and CO_2 detection†

Abigail A. Seddon, [a] Nathan S. Hill, [b] Osama El-Zubir,[d] Andrew Houlton,[d] R. John Errington, [a] Pablo Docampo[c] and Elizabeth A. Gibson *[a]

Chemiresitive sensing allows the affordable and facile detection of small molecules such as H_2O and CO_2. Herein, we report a novel class of Earth-abundant post transition metal substituted Keggin polyoxometalates (POMs) for chemiresistive sensing applications, with conductivities up to 0.01 S cm^{-1} under 100% CO_2 and 65% Relative Humidity (RH).

Recently, the use of POM anions as chemiresistive gas sensors has been explored.[1] Gas sensing is important for a wide range of applications such as the environmental and workplace monitoring of pollutants such as H_2S and ammonia,[2,3] sensing of H_2(g) for the widespread implementation of hydrogen fuel sources,[4] and within medical diagnostics for the identification of diseases.[5–7] Chemiresistive gas sensors are one of the most commercialised gas sensing technologies as they are simple to produce and utilise cheap and widely available materials.[1]

A chemiresistor is a material which, in response to changes in the chemical environment, will change its electrical resistance.[18] The direct interaction between the analyte and the material by hydrogen bonding, covalent bonding, or alternate intermolecular interactions is essential.[8] Simply, a basic device consists of a pair of interdigitated electrodes bridged by the sensing material. The difference in resistance between the two electrodes in the absence and presence of an analyte can be recorded. Traditional inorganic semiconductor materials including TiO_2 and SnO_2 and organic conductive polymers such as polyaniline are used for chemiresistive sensing applications.[9,10] The performance of inorganic semiconductor gas-sensitive materials is limited by rapid electron–hole recombination. POMs efficiently accept and store multiple electrons and protons, and these properties may reduce charge recombination between the electrodes. POMs can also be functionalised through their structure, elemental composition and cations, so their sensitivity to specific small molecules can be tuned.[11] Recent examples include a resistive humidity sensor based on a Keggin $H_3PMo_{12}O_{40}$-polypyrrole nanocomposite which was prepared by co-electrodeposition.[12] The sensor showed a rapid response and recovery time (1.9/1.1 seconds respectively at 98% RH), a sensing range of 11–98% RH, excellent durability, and repeatability with little hysteresis. POMs have been reported as efficient proton conductors,[13–15] as they have a decreased effective surface charge density as their negative charge is delocalised over peripheral oxygen atoms. A landmark study is that of Bourlinos and coworkers, who combined the acid-salt of $[PW_{12}O_{40}]^{3-}$ with a bulky PEG-containing quaternary ammonium cation, producing a liquid which exhibits high proton conductivity (10^{-3} S cm^{-1}).[15] Chemiresistive sensors for CO_2 detection have been evidenced in the literature, a Cu_3HIB_2 MOF has been reported to detect CO_2 with a limit of 400–2500 ppm, independent of humidity between 10–80%.[16] There are currently no reports of a similar system using POMs. In this communication, the conductivity of films with a novel series of post transition metal substituted POMs are measured to assess if they would be beneficial to use in sensing devices.

POMs were synthesised in acetonitrile *via* base degradation of $Na_3PW_{12}O_{40}$ with methanolic TBA(OH) to yield the lacunary species, followed by a substitution reaction with the appropriate post-TM salt as outlined in the (ESI†).[17–21] Simple chemiresistive devices were fabricated with two interdigitated indium tin oxide (ITO) coated electrodes bridged by the sensing material (Fig. S1, ESI†). The conductivity of the thin films was measured from 0–100% RH, displaying a large reversible increase in response with humidity from 2×10^{-6} S m^{-1} to 0.01 S m^{-1}, with a detection limit of 20–80% RH. Additionally, a

[a] *Energy Materials Laboratory, Chemistry, School of Natural and Environmental Sciences, Newcastle University, Newcastle upon Tyne, UK. E-mail: Elizabeth.gibson@newcastle.ac.uk*
[b] *School of Mathematics, Statistics, and Physics, Newcastle University, Newcastle upon Tyne, UK*
[c] *School of Chemistry, University of Glasgow, Glasgow, UK*
[d] *Chemical Nanoscience Labs, Chemistry, School of Natural and Environmental Sciences, Newcastle University, Newcastle upon Tyne, UK. E-mail: osama.el-zubir@newcastle.ac.uk, andrew.houlton@newcastle.ac.uk*

† Electronic supplementary information (ESI) available. See DOI: https://doi.org/10.1039/d3cc05660k

significant increase in conductivity was observed when these devices were measured in the presence of CO_2, indicating their use as chemiresistive sensors for the detection of H_2O and CO_2.

The device assembly is described in detail in the ESI.† Briefly, interdigitated electrodes were fabricated from ITO/glass substrates, with a channel etched between two electrodes. Thin films of POM were deposited on the electrodes, the film thickness was measured using atomic force microscopy (AFM), and the resistance was measured using 2-point current–voltage (*I*–*V*) sweeps. Two-point probe measurements are a useful tool to measure the conductivity of a material on a substrate with a low current output. Films of polyaniline (PANI) were also fabricated and measured as a reference for proton conduction. Measurements were undertaken in a humidity-controlled chamber, from 0–100% RH. Films of polymethyl methacrylate (PMMA, see ESI† for details) were also measured as a reference for film morphology, thickness, and for a reference in humidity measurements as its conductivity should not vary with humidity, proving differences in humidity observed were not due to water adsorbed on the surface.[22] The conductivity of the films was calculated using these data following the procedure outlined in the ESI.†

The AFM data on both the ITO electrode and on the glass are shown in Fig. 1 and Fig. S3–S6 (ESI†). These reveal the morphology of the film, average roughness (R_a) and film thickness, which was obtained by a line scan across a scratched mark. Some variation between samples in terms of roughness and particle size were observed as the substituent in the POM was changed. The film thickness varied significantly with the heterometal (Table 1). Films of $(TBA)_6[NaPW_{11}O_{39}]$ were the roughest and least homogeneous, with R_q an order of magnitude higher than for $(TBA)_4[BiPW_{11}O_{39}]$ (Table 1). The substituted POM films were smooth, with measured R_a values from 2.5 to 7.99 nm (Table 1). The same fabrication methodology was used for all POM films, so any differences in thickness and roughness are likely to be due to the different solubilities of the POMs, which influence the packing or interaction of the POM on the surface thus the way the film dries. Again, very small aggregates were observed on the ITO covered areas, and larger aggregates were observed in the ITO-free channel. This is likely due to the difference in surface charge between glass and ITO. The ITO surface is more positively charged,[23] so attracts the POM anions resulting in larger aggregates.

As expected, the PMMA films were uniform and smooth, and they had a thickness of *ca.* 200 nm (Fig. S3, ESI†).[16] For the thin film of $(TBA)_6[NaPW_{11}O_{39}]$, both large (2.5 μm) and small (< 500 nm) aggregates of POM were observed on the surface of the electrode (Fig. S4(c), ESI†) leading to a relatively high roughness (R_a = 21.51 ± 1.28 nm). In Fig. S4(b) (ESI†), the formation of lamellae can be observed on the part of the film over the ITO (non-active area). The film thickness was over 100 nm. Compared to $(TBA)_6[NaPW_{11}O_{39}]$ in Fig. S4 (ESI†), the

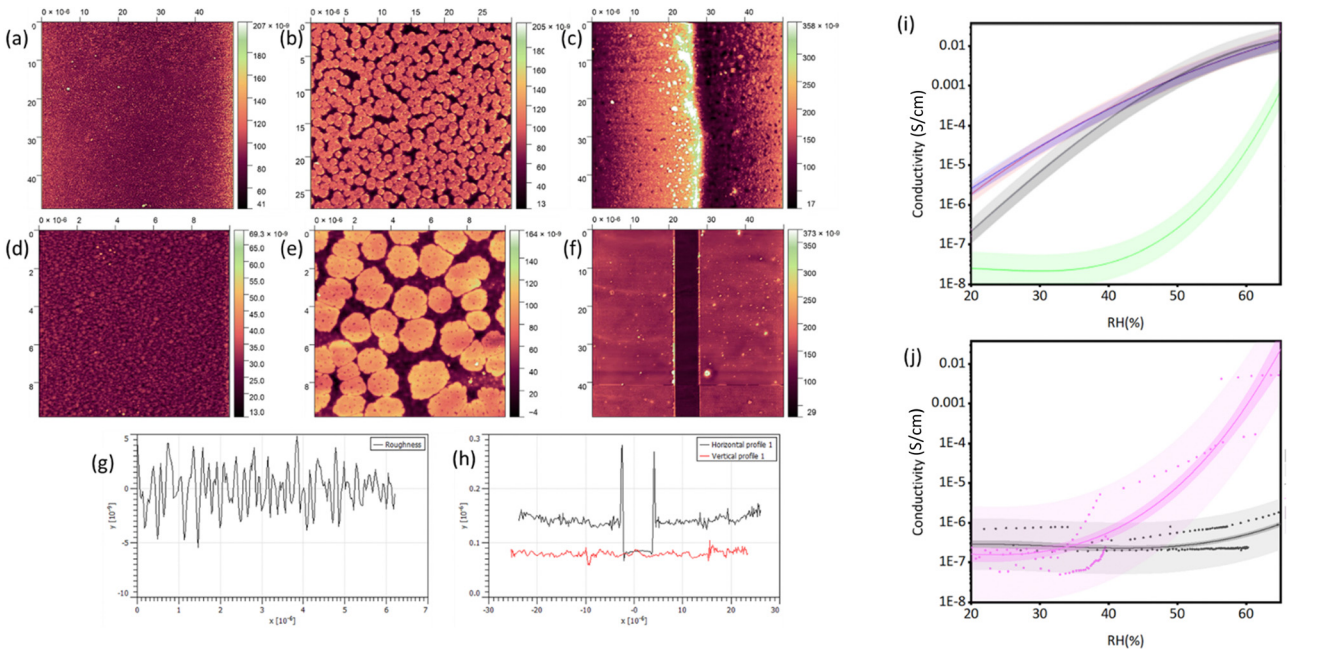

Fig. 1 (a)–(h) AFM images of a film of $(TBA)_4[BiPW_{11}O_{39}]$ deposited onto an interdigitated ITO electrode. (a) shows the morphology of the POM on the ITO edges, (b) POM on the electrode surface, (c) shows the electrode edge with observable POM aggregates, (d) higher magnification of the POM on the ITO edges. (e) POM aggregates in the electrode channel, (f) scratch used for thickness measurements, (h) profile of the scratch in (f) to obtain film thickness, and (g) shows the roughness of the electrode surface of (b). Colour bars show *z*-axis height of the surface (nm), whilst *x*- and *y*- axes show area analysed (μm) for (a)–(d). In (i), *y*-axis shows height (μm) and *x*-axis shows distance in the *x*-direction (μm). (j) and (k) Show conductivity (S cm^{-1}) *vs.* relative humidity (%) for substituted Keggin POMs. Shown are the results for thin films of: (i) humidity testing in air for all four POMs where $(TBA)_6[NaPW_{11}O_{39}]$ (black), $(TBA)_4[BiPW_{11}O_{39}]$ (red), $(TBA)_5[PbPW_{11}O_{39}]$ (blue), and $(TBA)_4[SbPW_{11}O_{39}]$ (green). (j) Response of thin film of $(TBA)_4[BiPW_{11}O_{39}]$ in the presence of CO_2 (pink) and N_2 (black). The shaded area shows the 95% confidence interval, and the solid line shows a 3rd order polynomial fit of the data.

Table 1 Morphology analysis of substituted POM interdigitated electrodes by AFM, and conductivity of the thin films measured at 0% RH. R_a = average roughness (nm), R_q = root mean square roughness (nm). Film thickness (nm) is measured by a step height scan

POM	Film thickness (nm)	R_a roughness (nm)	R_q roughness (nm)	Conductivity at 0% RH (S cm^{-2})
$(TBA)_6[NaPW_{11}O_{39}]$	147.7 ± 15.1	21.51 ± 1.28	29.47 ± 1.34	4.38×10^{-8}
$(TBA)_4[BiPW_{11}O_{39}]$	54.5 ± 3.3	2.50 ± 0.04	3.07 ± 0.05	1.22×10^{-7}
$(TBA)_5[PbPW_{11}O_{39}]$	878.4 ± 4.9	5.22 ± 0.06	6.48 ± 0.07	2.21×10^{-7}
$(TBA)_4[SbPW_{11}O_{39}]$	64.5 ± 2.3	7.99 ± 0.05	6.14 ± 0.06	1.93×10^{-8}

$(TBA)_4[BiPW_{11}O_{39}]$ POM produced significantly smoother and more homogenous films (Fig. 1). Aggregates were still observed on the electrode surface (Fig. 1(b)), but they were more consistent in size and distribution, roughly 1.5 μm in diameter. The POM aggregates were larger in size in the laser-etched electrode channel than on the remaining ITO coated areas (Fig. 1(a) and (d)). The film was also thinner, with the scratch height being around 50 nm. The thickest film, over 800 nm, was observed for $(TBA)_5[PbPW_{11}O_{39}]$ (Fig. S5(e), ESI†). These films were more homogenous than for $(TBA)_4[BiPW_{11}O_{39}]$ but contained many large aggregates on the surface causing increased roughness (Fig. S5(a) and (f), ESI†). Films of $(TBA)_4[SbPW_{11}O_{39}]$ (Fig. S6, ESI†) were similar in morphology to $(TBA)_6[NaPW_{11}O_{39}]$ (Fig. S4, ESI†), with many inhomogeneous aggregates of varying size on the electrode surface. The film thickness, 64.5 nm, was closer to that of $(TBA)_4[BiPW_{11}O_{39}]$.

Conductivity measurements were firstly benchmarked with a blank electrode (or glass), thick (200 nm) and thin (100 nm) films of PANI and PMMA (Fig. S7, ESI†). As expected, glass and PMMA showed no change with an increase in humidity, but the conductivity of PANI did change above *ca.* 40% humidity from 1×10^{-6} S m^{-1} at 35% RH to 0.003 S m^{-1} at 100% RH. This was expected as PANI is a known proton-conducting material.[24–27] Next, the measurements were performed with the POM electrodes and the data is presented in Fig. 1(i). Notably, the substituents play an important role on the conductivities observed at varying levels of RH in air. In Fig. 1(j) and (k), the conductivity of the films varies, with a different response observed depending on the substituent of the POM. The films of $(TBA)_6[NaPW_{11}O_{39}]$, $(TBA)_4[BiPW_{11}O_{39}]$, and $(TBA)_5[PbPW_{11}O_{39}]$ show responsiveness over a wider humidity range, and conductivity increases proportionally with humidity. POMs in solution exhibit proton conductivity *via* outer sphere proton-coupled electron-transfer mechanism.[28] In solid-state, proton conductivity occurs by either vehicular proton migration or proton-hopping for a high number of water molecules, or *via* the Grotthuss transfer mechanism for pseudoanhydrous or totally anhydrous proton transfer activity.[29,30] Overall, the highest conductivity at the highest humidity for the best performing devices was around 0.01 S cm^{-1} at 65% RH, which is significantly higher than previous literature reports (10^{-3} S cm^{-1}),[15] whilst operating at comparable humidity ranges. High proton conductivity arises *via* the Lewis acid centres, $Na^+/Bi^{3+}/Pb^{2+}$, and the POM acts as a Lewis base support. Differences observed in proton conductivity are related to the strength of the Lewis acid centre. Lewis acidity decreases from Bi(III) to Pb(II) and the Sb(III).[31,32] This has been shown previously with a crystalline composite of an Al^{3+}-oxocluster with a wheel-shaped POM, $[H_7P_8W_{48}O_{184}]^{33-}$.[33] Researchers reported ultrahigh proton conductivity of $>10^{-2}$ S cm^{-1}, which was attributed to the synergistic effect of the Lewis acid–Lewis base pairs which compensate for charge migration. This allows direct proton transfer from a Lewis acid (proton-donor) to a Lewis base (proton-acceptor) *via* the Grotthuss mechanism.[34] Consequentially, the use of substituted POMs as humidity sensing materials is demonstrated, whereby choice of substituent effects the response of the device. As the Lewis acidity of the substituent is increased, the sensitivity to RH is increased, especially in the mid-range.

At humidities above 40%, the conductivity of the $(TBA)_4[BiPW_{11}O_{39}]$ POM film increased substantially, up to 0.015 S m^{-2} at 65% humidity, when the air flowing over the sample was replaced with CO_2 (Fig. 1(j)). None of the other POM films measured showed a response to CO_2. Under N_2 rather than CO_2, at the same humidity, the conductivity was significantly lower, at around 10^{-6} S m^{-2}. The greater sensitivity of the POM to humidity in the presence of CO_2 indicates some interaction between the Bi in the POM and the CO_2. It is widely accepted that Lewis-acidic metals such as Cu(II), Pb(II), Bi(III), and Zn(II) promote CO_2 reduction.[32,35–38] The Bi(III)-POM is more readily reduced, or more readily accepts electron density, than the Pb(II)-POM species (Fig. S8–S11, ESI†),[39] therefore increasing sensitivity to CO_2. This demonstrates the potential use of substituted POM films as chemiresistive sensing materials for CO_2 detection. The different conductivity for $(TBA)_4[BiPW_{11}O_{39}]$ in humid air *vs.* humid N_2 (Fig. 1i–k) could be due to interactions with O_2 as well as CO_2 whereby the Lewis acidic site coordinates with Lewis-basic molecular oxygen.[40,41] Further work is needed to compare the selectivity of the system towards different small molecules and how this might be tuned by the substituents (*e.g.* Lewis acid–base).

In summary, a series of substituted lacunary Keggin POMs have been deposited onto interdigitated electrodes for the chemiresistive sensing of H_2O and CO_2, with clear differences observed in both film morphology and activity as the heterometal substituent is varied. This demonstrates the use of POMs in sensing devices, with a large increase in conductivity observed as humidity is increased. The observed response in reversible, with films being stable to multiple cycles of exposure to humidity and CO_2, as shown in Fig. S13 (ESI†). Further to this, $(TBA)_4[BiPW_{11}O_{39}]$ thin-film electrodes were tested as CO_2 sensors, again with promising results. A significant increase in current response was observed when the film was exposed to CO_2 in the presence of H_2O. However further work is needed to

assess the detection limits of CO_2, and the dependence of humidity on the response observed. This demonstrates the use of POMs within chemiresistive sensing technologies for the detection of small molecules as affordable and Earth-abundant materials with applications in product storage, medical testing, and workplace monitoring.

We are grateful to EPSRC for funding (EPRS1309X1, EP/S031170).

Conflicts of interest

There are no conflicts to declare.

Notes and references

1 P. Song and T. Wang, *ACS Sens.*, 2022, **7**, 3634–3643.
2 G. Barandun, M. Soprani, S. Naficy, M. Grell, M. Kasimatis, K. L. Chiu, A. Ponzoni and F. Güder, *ACS Sens.*, 2019, **4**, 1662–1669.
3 B. K. S. Reddy and P. H. Borse, *J. Electrochem. Soc.*, 2021, **168**, 057521.
4 W. T. Koo, H. J. Cho, D. H. Kim, Y. H. Kim, H. Shin, R. M. Penner and I. D. Kim, *ACS Nano*, 2020, **14**, 14284–14322.
5 N. Nasiri and C. Clarke, *Sensors*, 2019, **19**, 462–479.
6 T. Kuchmenko, A. Shuba, R. Umarkhanov and L. Lvova, *Chemosensors*, 2021, **9**, 116–132.
7 S. S. Shetty, A. Jayarama, I. Karunasagar and R. Pinto, *Mater. Today Proc.*, 2022, **55**, 122–126.
8 F.-G. Bănică, *Chemical Sensors and Biosensors*, John Wiley & Sons, Ltd, 2012, pp. 217–245.
9 B. Mondal and P. K. Gogoi, *ACS Appl. Electron. Mater.*, 2022, **4**, 59–86.
10 B. K. S. Reddy and P. H. Borse, *J. Electrochem. Soc.*, 2021, **168**, 057521.
11 A. Proust, B. Matt, R. Villanneau, G. Guillemot, P. Gouzerh and G. Izzet, *Chem. Soc. Rev.*, 2012, **41**, 7605–7622.
12 J. Miao, Y. Chen, Y. Li, J. Cheng, Q. Wu, K. W. Ng, X. Cheng, R. Chen, C. Cheng and Z. Tang, *ACS Appl. Nano Mater.*, 2018, **1**, 564–571.
13 T. Iwano, K. Shitamatsu, N. Ogiwara, M. Okuno, Y. Kikukawa, S. Ikemoto, S. Shirai, S. Muratsugu, P. G. Waddell, R. J. Errington, M. Sadakane and S. Uchida, *ACS Appl. Mater. Interfaces*, 2021, **13**, 19138–19147.
14 N. Ogiwara, T. Iwano, T. Ito and S. Uchida, *Coord. Chem. Rev.*, 2022, **462**, 214524.
15 A. B. Bourlinos, K. Raman, R. Herrera, Q. Zhang, L. A. Archer and E. P. Giannelis, *J. Am. Chem. Soc.*, 2004, **126**, 15358–15359.
16 R. J. Errington, in *Advances in Inorganic Chemistry*, eds. R. van Eldik and L. Cronin, Academic Press, 2017, vol. 69, pp. 287–336.
17 T. Izuagie, PhD thesis, Newcastle University, 2017.
18 R. J. Errington, in *Comprehensive Coordination Chemistry II*, ed. E. Constable, J. A. McClaverty and T. J. Meyer, Elsevier, Amsterdam, 2003, vol. 2, pp. 759–773.
19 R. J. Errington, in *Polyoxometalate Molecular Science*, ed. J. Borrás-Almenar, A. M. E. Coronado and M. Pope, Springer, Netherlands, II., 2003, vol. 1, pp. 55–78.
20 R. J. Errington, in *Polyoxometalate Chemistry: From Topology via Self-Assembly to Applications*, ed. M. T. Pope and A. Muller, Springer, Dordrecht, Dordrecht, 2001, vol. 1, pp. 1–22.
21 S. D. Wu and A. H. Chiou, *Sci. Rep.*, 2021, **11**, 1–12.
22 Md. R. Akanda, A. M. Osman, M. K. Nazal and Md. A. Aziz, *J. Electrochem. Soc.*, 2020, **167**, 037534.
23 L. Yue, Y. Zheng, Y. Xie, S. Liu, S. Guo, B. Yang and T. Tang, *RSC Adv.*, 2016, **6**, 68599–68605.
24 W. W. Focke and G. E. Wnek, *Conduction mechanisms in polyaniline (emeraldine salt)*, Elsevier, Sequoia S.A., 1988, vol. 256.
25 Z. Yang, D. H. Coutinho, R. Sulfstede, K. J. Balkus and J. P. Ferraris, *J. Membr. Sci.*, 2008, **313**, 86–90.
26 J. Stejskal, O. E. Bogomolova, N. V. Blinova, M. Trchová, I. Šeděnková, J. Prokeš and I. Sapurina, *Polym. Int.*, 2009, **58**, 872–879.
27 N. I. Gumerova and A. Rompel, *Chem. Soc. Rev.*, 2020, **49**, 7568–7601.
28 A. Martinelli, J. M. Otero-Mato, M. N. Garaga, K. Elamin, S. M. H. Rahman, J. W. Zwanziger, U. Werner-Zwanziger and L. M. Varela, *J. Am. Chem. Soc.*, 2021, **143**, 13895–13907.
29 Y. Zhou, J. Yang, H. Su, J. Zeng, S. P. Jiang and W. A. Goddard, *J. Am. Chem. Soc.*, 2014, **136**, 4954–4964.
30 P. Yang, M. Alsufyani, A. H. Emwas, C. Chen and N. M. Khashab, *Angew. Chem., Int. Ed.*, 2018, **57**, 13046–13051.
31 T. Ogawa, H. Ohashi, T. Tamaki and T. Yamaguchi, *Phys. Chem. Chem. Phys.*, 2013, **15**, 13814–13817.
32 C. J. Chang, Y. A. Lai, Y. C. Chu, C. K. Peng, H. Y. Tan, C. W. Pao, Y. G. Lin, S. F. Hung, H. C. Chen and H. M. Chen, *J. Am. Chem. Soc.*, 2023, **145**, 6953–6965.
33 J. Ramler and C. Lichtenberg, *Chem. – Eur. J.*, 2020, **26**, 10250–10258.
34 B. Chen and R. Neumann, *Eur. J. Inorg. Chem.*, 2018, 791–794.
35 Q. Wang, Z. Miao, Y. Zhang, T. Yan, L. Meng and X. Wang, *ACS Catal.*, 2022, **12**, 4016–4025.
36 H. Agarwala, X. Chen, J. R. Lyonnet, B. A. Johnson, M. Ahlquist and S. Ott, *Angew. Chem., Int. Ed.*, 2023, **62**, e202218728.
37 S. Fukuzumi, K. Ohkubo, Y. M. Lee and W. Nam, *Chem. – Eur. J.*, 2015, **21**, 17548–17559.
38 Q. Yang, W. Xu, S. Gong, G. Zheng, Z. Tian, Y. Wen, L. Peng, L. Zhang, Z. Lu and L. Chen, *Nat. Commun.*, 2020, **11**, 5478, DOI: **10.1038/s41467-020-19309-4**.